

Three-dimensionality in the wake of a rapidly rotating cylinder in uniform flow

A. Rao¹, J. S. Leontini^{1,†}, M. C. Thompson¹ and K. Hourigan^{1,2}

¹Fluids Laboratory for Aeronautical and Industrial Research (FLAIR), Department of Mechanical and Aerospace Engineering, Monash University, Melbourne, Victoria 3800, Australia

²Division of Biological Engineering, Monash University, Melbourne, Victoria 3800, Australia

(Received 25 February 2013; revised 23 April 2013; accepted 10 July 2013;
first published online 30 July 2013)

The flow around an isolated cylinder spinning at high rotation rates in free stream is investigated. The existence of two steady two-dimensional states is confirmed, as is the existence of a secondary mode of vortex shedding. The stability of the two steady states to three-dimensional perturbations is established using linear stability analysis. At lower rotation rates on the first steady state, two three-dimensional modes are confirmed, and their structure and curves of marginal stability as a function of rotation rate and Reynolds number are determined. One mode (named mode *E*) appears consistent with a hyperbolic instability in the wake, while the second (named mode *F*) appears to be a centrifugal instability of the flow very close to the cylinder surface. At higher rotation rates on the second steady state, a single three-dimensional mode due to centrifugal instability (named mode *F'*) is found. This mode becomes increasingly difficult to excite as the rotation rate is increased.

Key words: parametric instability, vortex flows, wakes/jets

1. Introduction

The flow associated with a rapidly rotating isolated cylinder in free stream is investigated. The flow is a function of two independent parameters: the Reynolds number $Re = UD/\nu$, and the normalized rotation rate $\alpha = \omega D/2U$. Here, U is the free stream velocity, D is the cylinder diameter, ν is the kinematic viscosity and ω is the rotation rate. The definition of α is such that it represents the ratio of the cylinder surface speed to the free stream velocity. When $\alpha = 0$ (no rotation), the well-studied problem of the flow past a rigid cylinder is recovered. With zero inflow (only rotation), the flow becomes that of a rotating cylinder in a quiescent fluid. As such, α acts as a type of bridge between these two fundamental flows, one wake-dominated, the other rotation-dominated. For the wake flows, the two-dimensional flows for $\alpha < 2.5$, and their subsequent loss of stability due to a range of three-dimensional instabilities, has been well described by Rao *et al.* (2013).

The pertinent results from that study to the current paper are as follows. Bénard-von Kármán-type vortex shedding was found to be suppressed for all Re for $\alpha > 1.9$, confirming and extending the findings of Mittal & Kumar (2003). On this steady

[†] Email address for correspondence: justin.leontini@monash.edu

flow, two three-dimensional instabilities were discovered using linear stability analysis, named mode *E* and mode *F*. Mode *E* was shown to have an aspect of hyperbolic instability occurring at the cusp of a single recirculation region in the wake. Mode *E* is stationary, representing the transition from a steady two-dimensional flow to a steady three-dimensional flow. Mode *F* was shown to be due to a centrifugal instability of the closed region encircling the cylinder. Unlike mode *E*, mode *F* varies with time, introducing a new frequency to the flow. This frequency appears to be associated with a travelling or modulated wave solution along the span of the cylinder.

A number of studies exist at higher rotation rates, particularly in the range $2.5 < \alpha < 6$. Mittal & Kumar (2003) covered this range for $Re = 200$ in detail, explicitly showing the existence of two steady solutions, with a hysteretic transition between the two in the range $4.8 \leq \alpha \leq 5.0$. These two solutions were differentiated by a change in length of the trailing shear layers that form the wake, and a movement of the hyperbolic point that forms in the flow where the fluid that orbits the cylinder rejoins the fluid that flows past. Using this movement of the hyperbolic point as a distinguishing feature, the results of Stojković, Breuer & Durst (2002) at $Re = 100$ also show evidence of a change in the steady solution in the range $4.5 \leq \alpha \leq 5.5$.

The study from Pralits, Brandt & Giannetti (2010) explicitly tracked the motion of this hyperbolic point in the flow as α was varied for $Re = 100$. The hyperbolic point was shown to typically move away from the cylinder across the flow, before also moving upstream (in fact moving beyond the central axis of the cylinder) for $\alpha > 5$. This paper then showed that near $\alpha = 5$, the flow changes between the two previously identified solutions. In fact, three stable solutions were identified as part of a careful continuation study.

As well as the two steady solutions, a periodic solution also exists at higher values of α . Stojković *et al.* (2003) identified this low-frequency single-sided vortex shedding over the range $60 \leq Re \leq 200$, and Mittal & Kumar (2003) showed that it stems from a Hopf bifurcation from the steady solution at lower rotation rates. This shedding regime, commonly known as *mode II shedding*, was observed in the recent experimental investigations of Kumar, Cantu & Gonzalez (2011). The two-dimensional DNS studies of El Akoury *et al.* (2008) showed that the range of rotation rates over which the mode II shedding was observed increased with Reynolds number.

A stability analysis and full three-dimensional DNS study at $Re = 200$ from Meena *et al.* (2011) showed that the flow was unstable to spanwise perturbations for $3.1 \leq \alpha \leq 5$, spanning the two previously established steady solutions. For $\alpha \leq 4.3$, the unstable modes were found to have purely real eigenvalues, and for $\alpha > 4.3$ (presumably a different base flow), the unstable modes obtained had complex eigenvalues. Interestingly, their three-dimensional simulations at $\alpha \simeq 3$ show the onset of centrifugal instabilities along the span of the cylinder, which Rao *et al.* (2013) demonstrated using stability analysis should have complex eigenvalues, or be temporally varying. Therefore, there seems to be some further work required to fully explain what occurs at these moderate values of α .

This paper confirms the existence of two steady solution states (here referred to as *steady state I* and *steady state II*), and the existence of a low-frequency vortex shedding for a small range of α for $Re > 50$. The stability of steady state I and steady state II to three-dimensional perturbations is then ascertained using linear stability analysis. Two three-dimensional modes are found to grow in steady state I; these are the modes identified as mode *E* and mode *F* in Rao *et al.* (2013). However, the shape of the curve of marginal stability in the (Re, α) plane is quite complicated for both modes, relating to very subtle changes in steady state I. A third three-dimensional

mode is found to grow in steady state II. Like mode F , this mode appears to be due to a centrifugal instability of the enclosed region of fluid orbiting the cylinder, and so it is named mode F' . The curve of marginal stability for this mode is quite simple, with Re_c increasing almost linearly with α .

2. Method and validation

2.1. Numerical method and stability analysis

The numerical method employed is identical to that described in Rao *et al.* (2013), and so only a brief overview is provided here. Simulations of the two-dimensional flow were conducted using a spectral-element method (Thompson, Hourigan & Sheridan 1996; Karniadakis & Sherwin 2005; Thompson *et al.* 2006; Leontini, Thompson & Hourigan 2007; Lo Jacono *et al.* 2010; Stewart *et al.* 2010). Typically, the time-dependent Navier–Stokes equations were integrated until the flow reached a steady state, or converged to a periodic oscillation. For cases where a steady solution was desired, but the flow was naturally periodic (where mode II shedding was observed), the steady spectral-element representation of the Navier–Stokes equations was solved using a Newton–Raphson method.

The stability of these steady solutions was then investigated using global linear stability analysis (Barkley & Henderson 1996; Schmid & Henningson 2001). Essentially, this method assesses whether linear perturbations, with a fixed spanwise wavelength λ , grow or decay over time. If they grow, the two-dimensional base flow is said to be unstable to three-dimensional perturbations at the given wavelength.

The two primary outputs of this method are the growth rate (which governs stability) and the mode shape associated with this growth rate. The growth rate is defined by a complex multiplier, μ , which can be interpreted as the ratio of the size of the perturbation from one time to the next. If $|\mu| > 1$, the perturbation grows and the base flow is unstable. Hence, when $|\mu| = 1$, the flow is said to be marginally stable. If μ has a non-zero imaginary component, the three-dimensional mode introduces a new frequency to the flow. If the base flow is steady (as the base flows of this paper are), then the three-dimensional mode is periodic in time. The complex growth rate σ is related to the multiplier $\mu = e^{\sigma T}$, where T is the period of sampling. For base flows that are periodic, the value of T is equal to the shedding period, while for steady base flows such as those studied in this paper, the value of T can be an arbitrary quantity.

The mode shape gives some indication of the regions of the base flow where perturbations grow, and therefore provides insight into the physical mechanism that leads to instability. A more detailed explanation is provided in Rao *et al.* (2013).

2.2. Resolution studies

Two meshes, M1 and M2, were employed to obtain the solutions for rotation rates below and above $\alpha = 5$, respectively. The distribution of the elements was more concentrated in the vicinity of the cylinder for M2, where large gradients in the flow are observed, particularly for high rotation rates. Both meshes used polynomial shape functions of seventh order and the boundaries were located $100D$ from the cylinder to avoid any blockage. Spatial resolution of the two domains was tested at the highest Reynolds number, $Re = 400$, at four different rotation rates. Lift and drag forces were found to vary by $<1\%$ with further increases in resolution, giving a high degree of confidence in the results obtained.

To validate these results, lift and drag coefficients at $Re = 200$ as a function of α are compared to the results of previous studies in table 1. Some discrepancy exists,

α	Padrino & Joseph (2006)		Mittal & Kumar (2003)		Present study	
	\bar{C}_d	\bar{C}_l	\bar{C}_d	\bar{C}_l	\bar{C}_d	\bar{C}_l
3	0.0123	-10.3400	0.0350	-10.3660	0.0397	-10.3335
4	-0.12401	-17.5820	-0.055	-17.5980	-0.0411	-17.5791
5	0.0107	-27.0287	0.1680	-27.0550	0.2169	-27.1139

TABLE 1. Variation of the time-averaged force coefficients (\bar{C}_d , \bar{C}_l) at the specified rotation rate (α) at $Re = 200$.

but there is also discrepancy between previously published values, particularly of the drag coefficient at $\alpha = 4$. The value of the drag coefficient at this point is very small, and is in fact negative, indicating that the rotating cylinder generates a small amount of thrust, as well as a more significant transverse force due to Magnus lift (Prandtl 1926). It is hypothesized that this thrust is highly dependent on the location of a hyperbolic point that forms in the flow, where fluid that orbits the cylinder and begins to flow upstream is brought to rest by fluid flowing downstream. Very small changes in this position can therefore result in very large (in relative terms) changes in the drag coefficient. In absolute terms, the change is very small, and so the comparison shown in table 1 provide further confidence that the simulations are accurate.

3. Results

The primary aim of this paper is the identification and description of the three-dimensional instabilities growing on the two steady base flow states: steady state I and steady state II. This allows the identification of the regions of the parameter space, here the (Re, α) plane, where the two-dimensional flow is expected to become unstable. These regions are determined by two factors: the regions of existence of the two-dimensional state; and the boundary of the unstable region, or the curve of marginal stability, for each of the three-dimensional modes. Therefore, the results of this paper are presented so that a map of the portion of the (Re, α) plane is presented first, in figure 1, illustrating these important factors. Following this, descriptions of the steady two-dimensional states, and the three-dimensional modes and their defining characteristics are presented.

3.1. Parameter space

Figure 1 presents a map of the portion of the (Re, α) plane studied. The regions of existence of each of steady state I and steady state II are marked by the grey and white backgrounds, respectively. Note that the ‘hard’ boundary between them should not be taken to mean that there is no overlap in these regions.

Pralits *et al.* (2010) explicitly showed that these two steady states are in fact a single continuous solution, at least at $Re = 200$, as α is varied. However, they showed that there is a loop with turning points at $\alpha = 5.17$ and $\alpha = 5.21$, meaning that for $5.17 < \alpha < 5.21$, there are in fact three possible steady states (figure 2*b* of Pralits *et al.* (2010) illustrates this very clearly). All three states can only be accessed by following the loop using a continuation method, even though they all belong to the same solution.

If a continuation method is not used, but α is simply slowly increased, there will be a discontinuous ‘jump’ as the turning point at $\alpha = 5.21$ is passed. Similarly, if α

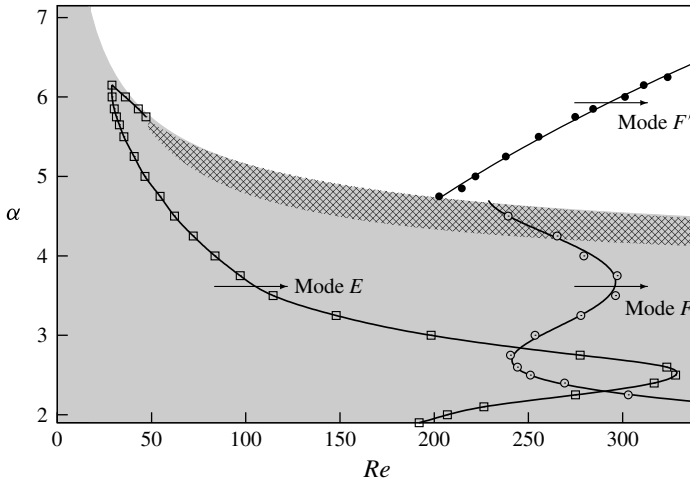


FIGURE 1. Regions of existence for steady state I (grey), steady state II (white), and the low-frequency vortex shedding mode (cross-hatched). Also marked are boundaries of marginal stability for the three-dimensional modes E ($-\square-$), F ($-\circ-$), and F' ($-\bullet-$) which grow on the two steady modes. The arrows crossing each marginal stability curve show the direction from stable to unstable flows. Three-dimensional modes marked with open symbols grow on steady state I (modes E and F), whereas solid symbols mark modes growing on steady state II (mode F'). Circular symbols mark three-dimensional modes caused by centrifugal instability (modes F and F').

is slowly decreased, there will be a ‘jump’ as the turning point at $\alpha = 5.17$ is passed. Hence, even though there is a single continuous solution, experiments (or simulations conducted by simple parameter scanning) will show a hysteretic transition between two steady states, as was found by Mittal & Kumar (2003). These two states are those named steady state I and steady state II in this paper, and are further described in § 3.2.

Following from this, it may be expected that the range of α between the two turning points is a function of Re , and that there may be a value of Re at which the two turning points coalesce into a kind of cusp point. This would eliminate the apparent hysteresis, but result in a discontinuous variation of the flow parameters (such as the drag force) as this point is crossed. The results shown in figure 2(a) for $\alpha = 6.15$, but the low Re -range $20 < Re < 60$, appear to show this.

Also shown (by the hashed region) in figure 1 is the region of existence of a low-frequency vortex shedding mode, previously identified by Mittal & Kumar (2003) to be a bifurcation from steady state I. The region identified here agrees well with the previous results of Stojković *et al.* (2003) and Pralits *et al.* (2010).

The curves of marginal stability of the three three-dimensional modes are marked with solid lines in figure 1. The points on each curve are the points at which $|\mu| = 1$ has been recorded. The small arrows crossing each of these curves indicates the direction from stable to unstable flows.

Two modes are shown to grow on steady state I: these are modes E and F , previously identified in Rao *et al.* (2013), which are marked with open symbols in figure 1. Mode E has been shown to likely be due to a hyperbolic instability at lower rotation rates (Rao *et al.* 2013). However, for these higher rotation rates, it is not clear that a hyperbolic mechanism is the only mechanism of growth. It may be that there is

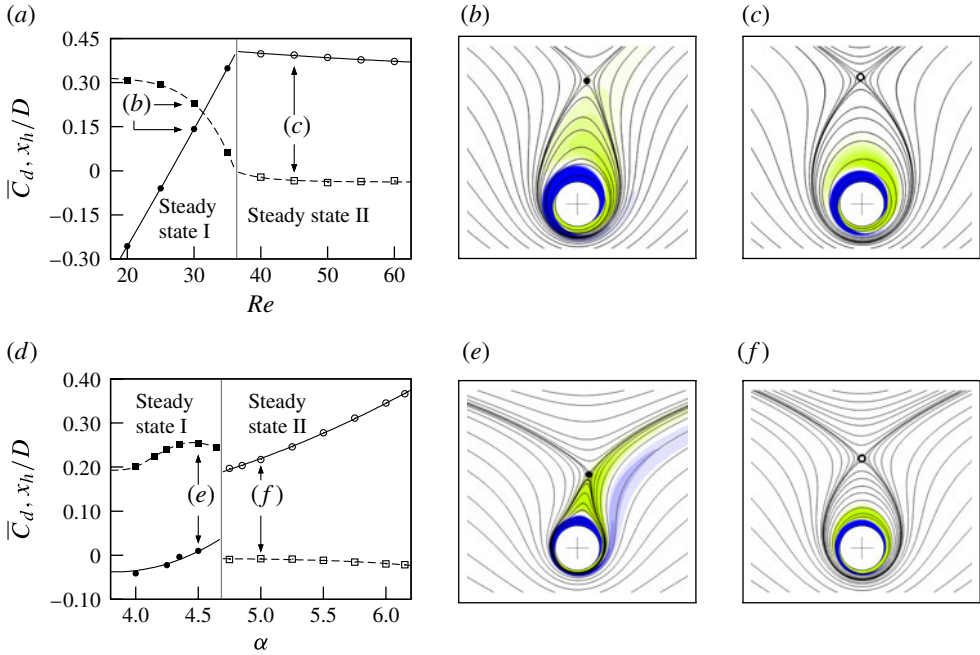


FIGURE 2. (Colour online) Delineation of the two steady states. (a–c) Constant $\alpha = 6.15$, increasing Re ; (d–f) constant $Re = 200$, increasing α . Both sets of data cross the boundary between steady state I and steady state II (the boundary marked by the vertical line). (a,d) Variation of the mean drag coefficient \bar{C}_d (■ and □ for mode steady state I and steady state II respectively) and the streamwise location of the hyperbolic point x_h (● and ○ for mode steady state I and steady state II respectively), with both variables showing a distinct change as this boundary is crossed. Panels (b) ($Re = 30$) and (e) ($\alpha = 4.5$) show examples of steady state I where the hyperbolic point is downstream of the cylinder centre. Panels (c) ($Re = 45$) and (f) ($\alpha = 5$) show examples of steady state II, where the hyperbolic point is upstream of the cylinder centre. All the flow images show streamlines and colour contours of vorticity at levels $\pm 3D/U$; cross-hairs mark the cylinder centre, circles mark the hyperbolic point location.

some cooperation between a centrifugal-type instability near the cylinder surface and a hyperbolic-type mechanism of amplification further downstream. Further investigation is required to completely understand the physical cause of instability for this mode. Mode F , however, appears to be due to a centrifugal instability of the layer of fluid at the cylinder surface (Rao *et al.* 2013). Both of these curves are of a reasonably complicated shape. Some explanation for this is given in §§ 3.3 and 3.4.

A single three-dimensional mode is found to grow on steady state II. This mode, like mode F , is due to a centrifugal instability, and so has been named mode F' . Like mode F , its curve of marginal stability is marked with filled circles in figure 1 and is much simpler than that for mode F , with Re increasing approximately linearly with α . Further details are provided in § 3.5.

3.2. Steady base flows

The two steady two-dimensional base flows, steady state I and steady state II, have been delineated in terms of two physical parameters: the streamwise location x_h of the hyperbolic point in the flow and the drag coefficient. For steady state I, the hyperbolic

point lies downstream of the centre of the cylinder, while for steady state II, the hyperbolic point is upstream of the centre of the cylinder. There is also a distinct change in drag coefficient moving from one solution to the other, clearly related to the change in location of this hyperbolic point and other associated changes in the flow structure. For example, steady state I has tail-like structures in the wake, while in steady state II, the shear layers wrap around the cylinder.

Plots of the streamwise location of the hyperbolic point and the drag coefficient, as the transition from steady state I to steady state II is crossed, are shown in figure 2. Also shown are examples of the steady flows on either side of the transition. Data for $\alpha = 6.15$ and varying Re are shown, as are data for $Re = 200$ and varying α . Both show the hyperbolic point moving from downstream to upstream as the transition occurs, as well as a distinct change in drag coefficient.

3.3. The mode E instability

Mode E was first described in Rao *et al.* (2013). There, it was shown that the stability multiplier μ was purely real, indicating that the mode introduces no new frequencies. It therefore represents a bifurcation from a steady two-dimensional flow to a steady three-dimensional flow. It was also attributed to a hyperbolic instability mechanism, in the high-strain region emanating from the hyperbolic point at the rear of a single recirculation region in the wake.

Images of mode E , progressing along the curve of marginal stability presented in figure 1, are shown in figure 3. A pertinent feature of the base flow (shown as streamlines in the images of figure 3) is that for $\alpha < 3$ (images a – e), the single recirculation region in the flow behind the body diminishes in size with increasing α . The hyperbolic point that forms at the rear of this recirculation region is brought closer to the cylinder, moving upstream and ‘down’ (transversely to the flow towards the wake centreline). For $\alpha > 3$ (images f – h), this recirculation region does not form. Increasing α sees the hyperbolic point continue to move upstream, but also move ‘up’ (transversely away from the wake centreline), away from the cylinder.

The structure of the perturbation (shown as colour contours of vorticity in the images of figure 3) also varies. When the recirculation region is present, the mode grows primarily in the high-strain region emanating from the hyperbolic point at its rear, the same structure as shown in Rao *et al.* (2013). However, for $\alpha > 3$ where the recirculation region has disappeared, the perturbation grows again near the hyperbolic point, but also in the enclosed layer of fluid near the cylinder surface. It is therefore plausible that at higher α , mode E is amplified by both hyperbolic and centrifugal instability mechanisms.

Inspection of figure 1 shows that as α is increased, Re_c (the value of Re at marginal stability for mode E) first increases, then decreases. The turning point is around $\alpha \simeq 2.5$, close to where the recirculation region disappears. For $\alpha > 2.5$, Re_c rapidly decreases. This is accompanied by an apparent exponential increase in the spanwise wavelength λ , as shown in figure 4. It should also be noted that at high $\alpha > 5.7$, the upper value of Re at which mode E is unstable is not at the boundary of existence of steady state I. Rather, the mode restabilizes before this boundary is reached.

3.4. The mode F instability

Mode F appears to be caused by a centrifugal instability of the layer of fluid close to the cylinder surface (Rao *et al.* 2013). At the higher values of α studied in this paper, the relationship between Re_c and α is reasonably complicated, with two turning points as shown in figure 1. The first of these occurs around $\alpha = 2.5$, again close to

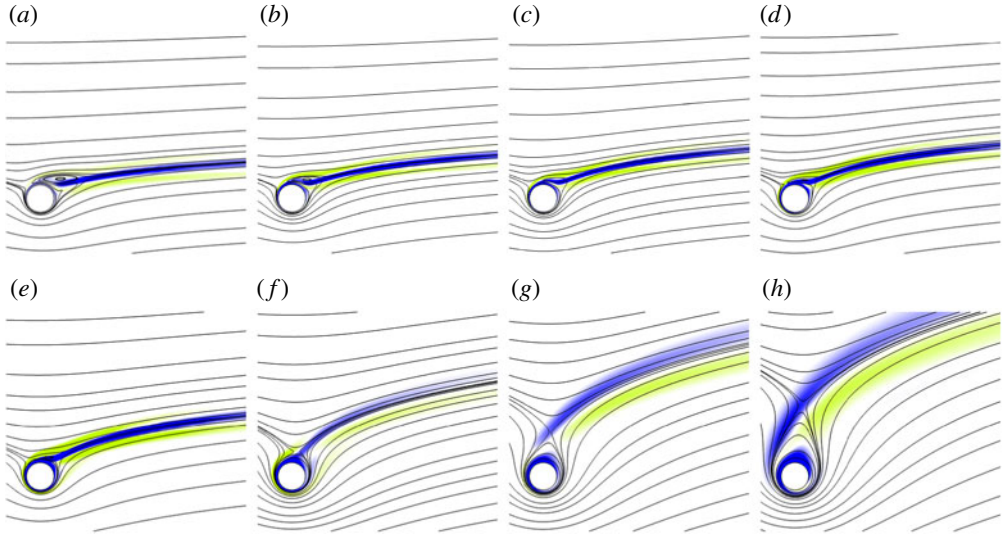


FIGURE 3. (Colour online) Spanwise perturbation vorticity contours of the mode E instability for (a) $\alpha = 2.1$, $Re = 240$, $\lambda/D = 1.8$; (b) $\alpha = 2.4$, $Re = 320$, $\lambda/D = 1.4$; (c) $\alpha = 2.6$, $Re = 340$, $\lambda/D = 1.4$; (d) $\alpha = 2.75$, $Re = 300$, $\lambda/D = 1.25$; (e) $\alpha = 3$, $Re = 220$, $\lambda/D = 1.2$; (f) $\alpha = 4$, $Re = 100$, $\lambda/D = 1.6$; (g) $\alpha = 5$, $Re = 50$, $\lambda/D = 4$ and (h) $\alpha = 6$, $Re = 30$, $\lambda/D = 9$. Contour levels vary between images as follows: (a–e) $\pm 0.100D/U$; (f) $\pm 0.250D/U$; (g) $\pm 0.010D/U$; (h) $\pm 0.005D/U$. Streamlines are overlaid over the contour plots. Flow is from left to right, with the cylinder spinning anticlockwise.

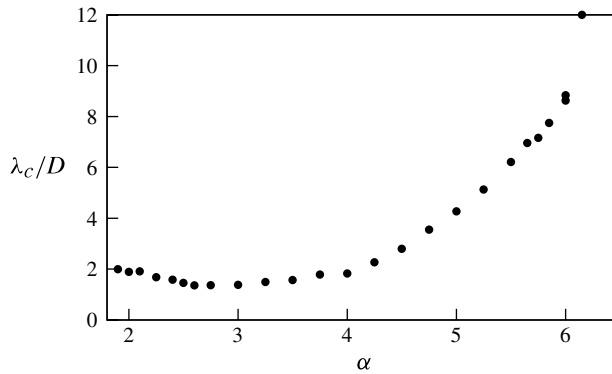


FIGURE 4. Variation of the critical spanwise wavelength with rotation rate for the mode E instability. The wavelength begins to increase exponentially around $\alpha = 2.5$, close to where the recirculation region in the wake disappears.

the value where the recirculation region in the wake disappears. The second occurs close to $\alpha = 3.8$. Therefore, the stability behaviour of mode F can be broken into three ranges of α : $\alpha < 2.5$, where Re_c decreases with increasing α ; $2.5 \leq \alpha < 3.8$, where Re_c increases with α ; and $3.8 \leq \alpha < 4.8$, where Re_c again decreases with increasing α before steady state I ceases. This behaviour can be explained by considering the centrifugal mechanism of instability.

Initially ignoring viscous effects, for a flow to be centrifugally unstable, curved streamlines are required, with higher angular momentum fluid on the inside of the curve than outside (Rayleigh 1917; Drazin 2004). This occurs in the enclosed region of fluid at the cylinder surface. The wavelength of the instability scales as the thickness of the layer of fluid, which is centrifugally unstable (Taylor 1923; Drazin 2004). Therefore, thinner boundary layers imply shorter wavelengths. Viscosity now plays a role, in that it more effectively dampens short wavelengths than long wavelengths, so that the flow should be stable until higher Re . Therefore, thinner boundary layers imply shorter wavelengths which imply higher Re_c .

Figure 5(a*i*) shows the approximate thickness of the centrifugally unstable region (defined as the region with tangential velocity decreasing outwards at the rear of the cylinder) as a function of α along the curve of marginal stability for mode F . Figure 5(a*ii*) shows the variation of the most unstable wavelength. The figure shows that the wavelength appears to be proportional to the boundary layer thickness, which has turning points at similar values of α as Re_c shown in figure 1.

Figure 5(a*iii*) is the predicted frequency of mode F along the curve of marginal stability. As stated in §2.1, if the imaginary component of μ is non-zero, a new frequency is introduced by the three-dimensional mode. This frequency (non-dimensionalized by the U and D to become a Strouhal number) can be calculated from the complex multiplier as $St_{3D} = \tan^{-1}(\mu_{imag}/\mu_{real})/(2\pi T)$. Figure 5 shows that this frequency is approximately inversely proportional to the boundary layer thickness.

Rao *et al.* (2013) showed that the frequency of mode F is governed by the time taken for a ‘packet’ of perturbation to orbit the cylinder twice. The orbital speed has been shown to be dictated by the orbital speed of one particular streamline around the cylinder. The position (or radius) of this streamline is the radius of the cylinder plus some proportion of the boundary layer thickness. If this proportion remains constant, as the boundary layer thickness is reduced, this ‘governing’ streamline will move closer to the cylinder surface, and therefore might be expected to have a higher speed, resulting in a higher frequency. The results here imply that this mechanism is at work for mode F .

3.5. The mode F' instability

Mode F' is similar in structure and behaviour to mode F , except that it grows on steady state II. As for mode F , this mode is caused by a centrifugal instability of the layer of fluid adjacent to the cylinder surface. It appears to be the only three-dimensional instability of steady state II. This is most likely due to the fact that the wake region is much less significant with the onset of steady state II, so only the instability mechanisms that act on the surface layer are viable.

In a manner similar to mode F , mode F' introduces a new frequency that is governed by the time it takes for a perturbation packet to orbit the cylinder twice. Figure 6 shows a sequence of eight images of the perturbation vorticity field of mode F' taken over one period. Images (a–d) (covering the first half-period) are mirrored by images (e–h) (covering the second half-period), except for a change in sign. The orbiting nature of the perturbation can be deduced by noting the position of the predominantly green (light) blob in (a–d), and the position of the predominantly blue (dark) blob in (e–h).

Unlike mode F , the progression of mode F' with increasing α is reasonably simple. With increasing α , Re_c increases essentially linearly. Figure 5(b*i*) shows that the boundary layer thickness decreases approximately linearly. As for mode F , figures 5(b*ii*) and 5(b*iii*) show that the critical wavelength is proportional to the

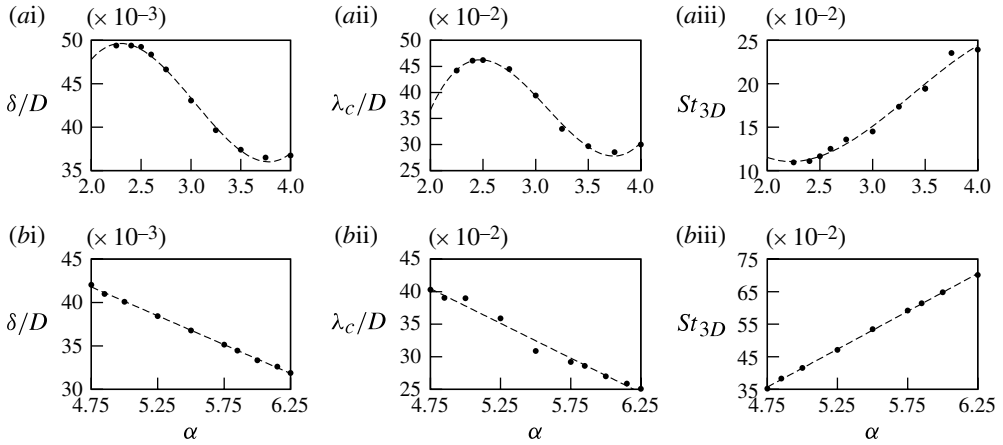


FIGURE 5. (i) Boundary layer thickness δ/D , (ii) critical wavelength λ_c/D , (iii) Strouhal number of the three-dimensional mode, St_{3D} , for (a) mode F and (b) mode F' , all measured along the relevant marginal stability curve (note that Re is also a function of α as shown in figure 1). Dots (\bullet) are measurements, dashed lines (---) are approximated trend lines. Both modes are centrifugally unstable, and the figures show that in both cases λ_c/D is approximately proportional to δ/D , and St_{3D} is approximately inversely proportional to δ/D .

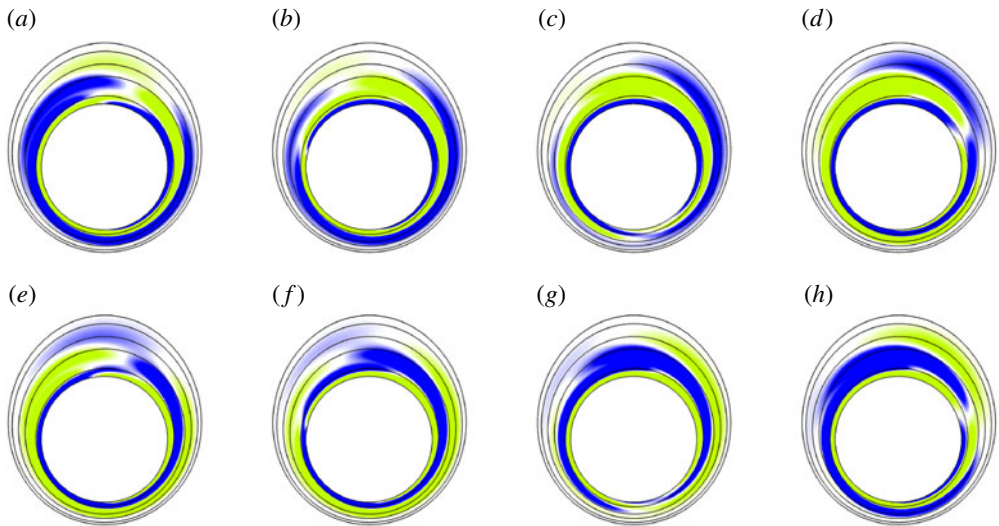


FIGURE 6. (Colour online) Spanwise perturbation vorticity contours of the mode F' instability over one period of shedding at $\alpha = 6$, $Re = 320$ and $\lambda/D = 0.3$, with streamlines in the vicinity of the cylinder overlaid: (a) $T = 0, T$; (b) $T = T/8$; (c) $T = 2T/8$; (d) $T = 3T/8$; (e) $T = 4T/8$; (f) $T = 5T/8$; (g) $T = 6T/8$; (h) $T = 7T/8$.

boundary layer thickness, and the frequency is approximately inversely proportional to the boundary layer thickness. This implies that the same argument presented in § 3.4 for the scaling of the wavelength and frequency for mode F also applies for mode F' .

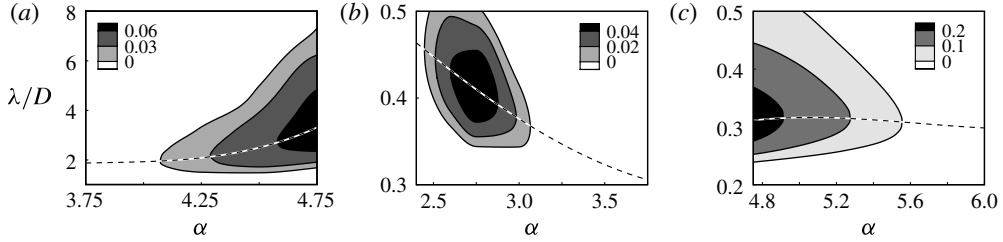


FIGURE 7. Contours of positive growth rates ($\sigma \geq 0$) as a function of α and λ/D for (a) mode E at $Re = 80$, (b) mode F at $Re = 260$ and (c) mode F' at $Re = 260$. In all the plots, the solid lines (—) and shaded contours represent levels of σ , and the dashed line (---) shows the value of λ/D at which the maximum growth rate occurs for each α . The plots show that a wide range of wavelengths can be unstable, and this range is not simply centred around the value of λ/D at maximum growth.

The constant decrease in the boundary layer thickness with increasing α and the constant increase in Re_c imply that as $\alpha \rightarrow \infty$, the boundary layer thickness approaches zero, and $Re_c \rightarrow \infty$.

3.6. Variation of the wavelength of all modes with rotation rate

While the stability analysis typically predicts a fastest-growing wavelength, for parameters beyond marginal stability, there is a range of wavelengths that become unstable for a given mode. If Re is held constant, this range is defined by the area enclosed by the contour of marginal stability (where the growth rate $\sigma = 0$) in the α, λ plane. Figure 7(a) shows this contour for mode E at $Re = 80$. Figures 7(b) and 7(c) show this contour for modes F and F' at $Re = 260$. The plots of figure 7 also show contours at other positive values of σ , where the base flow is unstable to the given mode, and a dashed line showing the value of λ/D at which the growth is maximum for a given α .

The figure shows that for all modes, the range of unstable wavelengths initially increases quickly once the critical value of α (the value at which the flow first becomes unstable) is crossed. For mode E , this occurs at $\alpha \simeq 4.1$ as α is increased. For mode F , this occurs both at $\alpha \simeq 2.4$ as α is increased, and $\alpha \simeq 3.1$ as α is decreased (the complicated shape of the marginal stability curve for mode F shown in figure 1 shows that the growth rate should first increase, then decrease with increasing α). For mode F' , this occurs at $\alpha \simeq 5.6$ as α is decreased. Also, this range is not always centred around the value of λ/D at which the growth is at a maximum. This is particularly clear for mode E , where the value of λ/D at maximum growth is towards the lower end of the range of unstable wavelengths, particularly for higher values of α , as shown in figure 7(a). This is despite λ/D at maximum growth increasing with increasing α .

These results indicate that, once the flow is unstable, there is a multitude of wavelengths that can be excited. The wavelength of the eventual saturated flow may not match the wavelength predicted to have the highest linear growth. Some caution therefore needs to be taken when using the stability analysis results of this paper to identify modes in experimental or direct numerical simulation settings, particularly far beyond the marginal stability point.

4. Conclusions

The stability of the flow past a rotating cylinder at higher rotation rates in a free stream has been investigated using linear stability analysis. The existence of two steady states has been confirmed. The first of these states, named steady state I, has been confirmed to be unstable to two three-dimensional modes. The first, mode E is essentially an instability of the wake, yet shows some possible dependence on a centrifugal instability mechanism with increasing rotation rates. The second, mode F , is purely due to centrifugal instability, and the variation of Re_c for this mode has been explained by considering this. The second steady state, steady state II, occurs at higher rotation rates and has been shown to be unstable to a single three-dimensional mode, mode F' . This mode is also due to a centrifugal instability.

Acknowledgements

The authors acknowledge computing-time support from the Victorian Life Sciences Computation Initiative (VLSCI), the National Computational Infrastructure (NCI) and the Monash Sungrid, Clayton. The authors acknowledge financial support from Australian Research Council (ARC) grants DP0877327, DP110102141 and DP130100822. A.R. acknowledges the financial support of Monash University through a Postgraduate Publication Award. J.S.L. acknowledges the financial support of the ARC through an Australian Postdoctoral Fellowship.

REFERENCES

- BARKLEY, D. & HENDERSON, R. D. 1996 Three-dimensional Floquet stability analysis of the wake of a circular cylinder. *J. Fluid Mech.* **322**, 215–241.
- DRAZIN, P. G. 2004 *Hydrodynamic Stability*, 2nd edn. Cambridge University Press.
- EL AKOURY, R., BRAZA, M., PERRIN, R., HARRAN, G. & HOARAU, Y. 2008 The three-dimensional transition in the flow around a rotating cylinder. *J. Fluid Mech.* **607**, 1–11.
- KARNIADAKIS, G. E. & SHERWIN, S. J. 2005 *Spectral/hp Methods for Computational Fluid Dynamics*. Oxford University Press.
- KUMAR, S., CANTU, C. & GONZALEZ, B. 2011 Flow past a rotating cylinder at low and high rotation rates. *Trans. ASME: J. Fluids Engng* **133** (4), 041201.
- LEONTINI, J. S., THOMPSON, M. C. & HOURIGAN, K. 2007 Three-dimensional transition in the wake of a transversely oscillating cylinder. *J. Fluid Mech.* **577**, 79–104.
- LO JACONO, D., LEONTINI, J. S., THOMPSON, M. C. & SHERIDAN, J. 2010 Modification of three-dimensional transition in the wake of a rotationally oscillating cylinder. *J. Fluid Mech.* **643**, 349–362.
- MEENA, J., SIDHARTH, G. S., KHAN, M. H. & MITTAL, S. 2011 Three-dimensional instabilities in flow past a spinning and translating cylinder. In *IUTAM Symposium on Bluff Body Flows*, pp. 59–62. Indian Institute of Technology Kanpur.
- MITTAL, S. & KUMAR, B. 2003 Flow past a rotating cylinder. *J. Fluid Mech.* **476**, 303–334.
- PADRINO, J. C. & JOSEPH, D. D. 2006 Numerical study of the steady-state uniform flow past a rotating cylinder. *J. Fluid Mech.* **557**, 191–223.
- PRALITS, J. O., BRANDT, L. & GIANNETTI, F. 2010 Instability and sensitivity of the flow around a rotating circular cylinder. *J. Fluid Mech.* **650**, 513–536.
- PRANDTL, L. 1926 *Application of the 'Magnus Effect' to the Wind Propulsion of Ships*. National Advisory Committee for Aeronautics.
- RAO, A., LEONTINI, J., THOMPSON, M. C. & HOURIGAN, K. 2013 Three-dimensionality in the wake of a rotating cylinder in a uniform flow. *J. Fluid Mech.* **717**, 1–29.
- RAYLEIGH, J. W. STRUTT, LORD 1917 On the dynamics of revolving fluids. *Proc. R. Soc. Lond. Ser. A* **93**, 148–154.
- SCHMID, P. J. & HENNINGSON, D. S. 2001 *Stability and Transition in Shear Flows*. Springer.

- STEWART, B. E., THOMPSON, M. C., LEWEKE, T. & HOURIGAN, K. 2010 The wake behind a cylinder rolling on a wall at varying rotation rates. *J. Fluid Mech.* **648**, 225–256.
- STOJKOVIĆ, D., BREUER, M. & DURST, F. 2002 Effect of high rotation rates on the laminar flow around a circular cylinder. *Phys. Fluids* **1** (9), 3160–3178.
- STOJKOVIĆ, D., SCHÖN, P., BREUER, M. & DURST, F. 2003 On the new vortex shedding mode past a rotating circular cylinder. *Phys. Fluids* **15** (5), 1257–1260.
- TAYLOR, G. I. 1923 Stability of a viscous liquid contained between two rotating cylinders. *Phil. Trans. R. Soc. Lond. Ser. A* **223**, 289–343.
- THOMPSON, M. C., HOURIGAN, K., CHEUNG, A. & LEWEKE, T. 2006 Hydrodynamics of a particle impact on a wall. *Appl. Math. Model.* **30**, 1356–1369.
- THOMPSON, M. C., HOURIGAN, K. & SHERIDAN, J. 1996 Three-dimensional instabilities in the wake of a circular cylinder. *Exp. Therm. Fluid Sci.* **12** (2), 190–196.